Heat Transfer and Fluid Flow in Plasma Spraying

N. EL-KADDAH, J. McKELLIGET, and J. SZEKELY

A mathematical model is developed to describe the plasma spray process in which particular attention is paid to the fluid flow and temperature fields in the plasma jet, the plasma/particle interaction, and the heat transfer phenomena associated with the deposition process. On the basis of the heat transfer analysis it was possible to define the limiting conditions for satisfactory operation of the deposition process in terms of basic process variables. For high deposition rates, high levels of superheat, and low thermal conductivity of the deposit, the limiting condition is set by the rate at which heat may be removed by the substrate. For large particle sizes and materials with high melting points the limiting condition is determined by the need to transfer sufficient thermal energy to the particles so that they arrive at the substrate in a fully molten state. Wherever possible, the model predictions were compared with experimental measurements and good agreement was obtained.

I. INTRODUCTION

FOR a considerable time plasma spraying has been a well-accepted technology for the production of thermal barrier and corrosion resistant coatings for critical applications. While the actual technology is well documented, up to the present time the scientific basis of these operations has been concerned with the structural characterization of the deposits rather than with the heat transfer and fluid flow aspects of the system. As plasma spraying is being extended to a broader range of critical applications, as well as for the production of massive deposits, the quantitative description of the thermal history of the deposit and the actual limiting conditions of satisfactory operation are becoming progressively important.

Figure 1 shows a sketch of a typical plasma spraying system. It is seen that solid particles are introduced into a plasma jet issuing from a plasma gun. During their flight the particles become heated, molten, and impinge upon the substrate to be coated, where they solidify. In an ideal operation the particles will become fully molten, but not overheated, during their flight and arrive at the substrate surface with a sufficiently high velocity that, upon impact and subsequent solidification, a fully coherent, nonporous coating is produced.

On the basis of purely physical reasoning one may envisage two limiting cases of operation:

1. When insufficient thermal energy is transferred to the solid particles so that they are not fully molten upon arrival at the substrate surface, an unacceptable or porous deposit may result.
2. When the rate of heat transfer to the substrate is excessively rapid, solidification of the molten particles cannot occur, leading to the formation of a liquid pool at the substrate surface. This is also an unacceptable condition.

In practice, a further fine tuning of these operations is advisable, since it is desirable to prevent the excessive volatilization of the particles, and in order to provide proper bonding between the substrate and the deposit a certain preferred thermal history should be obtained, while at the same time ensuring that solidification will be sufficiently rapid.

The proper quantitative representation of this system, which is necessary if excessive empiricism is to be avoided, must address four principal areas of interest:

1. the fluid flow and thermal characteristics of the plasma;
2. the trajectories, and hence the residence times, of the particles;
3. the plasma/particle heat transfer; and
4. the solidification of the deposit. This will be determined by both the rate of heat and material transfer to the deposit and by the conductive heat transfer into the substrate.

It should be noted that individual aspects of this problem have been studied to varying extents but that these component parts have yet to be combined into a comprehensive model.

Heat transfer and fluid flow in plasmas have been studied both experimentally[1,2] and analytically.[3,4] The early work employed the laws of classical electrodynamics,[5] while more recent efforts have made use of computational techniques employing turbulence models.[6] The predictions based on these models[6] were found to be in reasonable agreement with the careful measurements of Fauchais and co-workers.[1] In the past, the theoretical calculations have been restricted to the case of a free plasma flame in the absence of a target. The current paper is the first to deal with the physically more meaningful situation of an impinging jet flow.

The situation pertaining to particle trajectories and plasma/particle heat transfer closely parallels that of heat and fluid flow in plasma systems in the absence of particles in that the early approximate analytical procedures are being supplanted by a more sophisticated numerical approach.[1-4] As a result of this latter work one may now, with some confidence, perform calculations regarding both the residence time and the temperature histories of the solid particles suspended in the plasma.

In contrast to the work that has been done on the characterization of the plasma jets and the associated particles, the heat transfer phenomena associated with the deposition process have received very little attention up to the present. The principal reason for this is probably not so much due to the complexity of the heat transfer problem but rather due to the lack of information pertaining to the plasma

N. EL-KADDAH is Associate Professor, Cairo University and is on sabbatical leave at Massachusetts Institute of Technology; J. McKELLIGET is Visiting Scientist in the Department of Materials Science and Engineering; J. SZEKELY is Professor of Materials Engineering and Associate Director, Center for Materials Processing. All are at the Massachusetts Institute of Technology, Cambridge, MA 02139.

Manuscript submitted November 15, 1982.

behavior, most of which has only recently reached the open literature in a readily accessible form.

II. MODEL FORMULATION

A. *Plasma Flame Model*

For the system sketched in Figure 1 the plasma stream leaves the torch in the form of a turbulent, compressible jet of hot ionized gas. The problem of practical importance is to calculate the velocity and temperature fields in the gas downstream of the torch for a given set of initial conditions at the exit. In general, the gas velocity and temperature at the exit from the torch are not known but they may be estimated from simple mass and energy conservation principles applied to the working gas of the torch since the torch power and volumetric flowrate of gas are usually given. For simplicity it was assumed that the radial profiles of temperature and velocity at the exit were 'top hat' distributions and that there were no energy losses from the torch.

The velocity and temperature fields downstream of the torch exit were calculated from the appropriate equations of mass, momentum, and energy conservation which may be expressed in two-dimensional form by assuming that the arc is symmetrical about the torch axis and that the flow is time independent. The equations take the following form:

equation of mass continuity:

$$\frac{\partial}{\partial z}(\rho_g u_g) + \frac{1}{r}\frac{\partial}{\partial r}(\rho_g r v_g) = 0 \qquad [1]$$

conservation of axial momentum:

$$\frac{\partial}{\partial z}(\rho_g u_g^2) + \frac{1}{r}\frac{\partial}{\partial r}(\rho_g r v_g u_g) = \frac{-\partial P}{\partial z} + \frac{2\partial}{\partial z}\left(\mu_{\text{eff}}\frac{\partial u_g}{\partial z}\right) + \frac{1}{r}\frac{\partial}{\partial r} \cdot \left\{r\mu_{\text{eff}}\left(\frac{\partial u_g}{\partial r} + \frac{\partial v_g}{\partial z}\right)\right\} \qquad [2]$$

conservation of radial momentum:

$$\frac{\partial}{\partial z}(\rho_g u_g v_g) + \frac{1}{r}\frac{\partial}{\partial r}(\rho_g r v_g^2) = \frac{-\partial P}{\partial r} + \frac{\partial}{\partial z}\left\{\mu_{\text{eff}}\left(\frac{\partial v_g}{\partial z} + \frac{\partial u_g}{\partial r}\right)\right\} + \frac{2}{r}\frac{\partial}{\partial r}\left(\mu_{\text{eff}}\frac{r\partial v_g}{\partial r}\right) - \frac{2v_g}{r^2}\mu_{\text{eff}} \qquad [3]$$

conservation of energy:

$$\frac{\partial}{\partial z}(\rho_g u_g T_g) + \frac{1}{r}\frac{\partial}{\partial r}(\rho_g r v_g T_g) = \frac{\partial}{\partial z}\left(\frac{\mu_{\text{eff}}}{\sigma_T}\frac{\partial T_g}{\partial z}\right) + \frac{1}{r}\frac{\partial}{\partial r}\left(\frac{\mu_{\text{eff}}}{\sigma_T}\frac{r\partial T_g}{\partial r}\right) - \frac{S_R}{C_g} \qquad [4]$$

In these equations z is the axial distance from the torch exit in the direction of axial gas flow, and r is the radial distance of a point from the axis of symmetry.

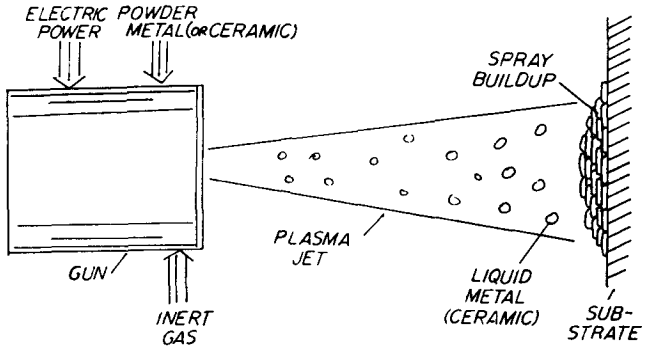

Fig. 1—Schematic representation of plasma spraying process.

In Eq. [4] compressibility effects and viscous heat generation have been neglected. The term S_R represents an approximate optically thin radiation loss per unit volume.

The essentially turbulent nature of the flow was described by an effective viscosity, μ_{eff}, which was calculated from the well-known k-ε two equation turbulence model.[7] (See Appendix 1.)

The boundary conditions are given as follows:

At the axis of symmetry ($r = 0$),

$$v_g = \partial u_g/\partial r = \partial T_g/\partial r = 0 \qquad [5]$$

At the solid surfaces,

$$v_g = u_g = 0 \qquad [6]$$

$$T_g = 500\ \text{K} \qquad [7]$$

At the torch exit ($z = 0$, $r \leq R_0$)

$$v_g = 0, \qquad u_g = u_0, \qquad T_g = T_0 \qquad [8]$$

At large distances from the axis of symmetry ($r \rightarrow \infty$)

$$\frac{\partial}{\partial r}(\rho_g r v_g) = 0, \qquad \frac{\partial u_g}{\partial r} = 0 \qquad [9]$$

The heat transfer from the arc to the solid target was calculated using standard wall function techniques.[7] In the immediate impingement zone the heat fluxes to the target were calculated using a heat transfer correlation obtained from re-entry problem studies[5]

$$q_t = h(C_{g,b}T_{g,b} - C_{g,w}T_{g,w}) \qquad [10]$$

where q_t is the heat flux from the plasma jet to the target and h is given by

$$h = \frac{0.915}{\sigma_{T,g,w}}\left\{\frac{\rho_{g,b}\mu_{g,b}}{\rho_{g,w}\mu_{g,w}}\right\}^{0.43}\left\{\rho_{g,w}\mu_{g,w}\frac{v_{g,b}}{r}\right\}^{0.5} \qquad [11]$$

In Eqs. [10] and [11] $\sigma_{T,g}$ is the laminar Prandtl number of the gas, and the subscripts w and b refer to the wall and the edge of the boundary layer in the plasma, respectively.

The value of 500 K assigned to the temperature of the anode in Eq. [7] is arbitrary and has little effect on the calculated plasma temperature field. This value is allowed to vary when the temperature fields in the target are calculated.

The temperature dependent values of density, molecular viscosity, thermal conductivity, and specific heat were taken from the tabulated data of Liu.[8] The radiation loss per unit volume for argon was taken from the measured values of Evans and Tankin.[9]

The governing equations were solved numerically using the techniques described by Pun and Spalding.[10] A 20 × 20 finite difference grid was used and a typical run required about 150 seconds CPU time on the IBM 370 computer at Massachusetts Institute of Technology. Convergence of the iterative numerical scheme was achieved when appropriate convergence criteria were satisfied and when overall mass and energy balances were satisfied to an accuracy of 90 to 95 pct.

B. *Particle History Model*

If it is assumed that the presence of the particles does not disturb the plasma flow field, then the motion of the particles in the axial direction is given by the Basset-Boussinesq-Oseen equation.

$$\frac{d}{dt}(M_p u_p) = \frac{-\pi}{8} D_p^2 \rho_{g,e} C_{D'} |u_p - u_g| (u_p - u_g) - (1.5\pi^{0.5} D_p^2) \int_0^t (\mu_{g,av} \rho_{g,av})^{0.5} \times \left\{ \frac{d}{dt'} (u_p - u_g) \right\} (t - t')^{-0.5} dt' \quad [12]$$

In this equation the first term on the right-hand side is the drag force acting on the particle and the second is a Basset history term representing the time dependent nature of the boundary layer around the particle. The history term is necessary since for plasma systems particle residence times are comparable with boundary layer relaxation times (≃1 ms). Boulos and Gauvin[4] report that the history term should be retained for particle diameters greater than 30 μm. A similar equation but with the history term omitted was used to calculate the radial motion of the particle. The added mass term has been neglected from Eq. [12] since the density of the particles is much greater than the density of the plasma.

The drag coefficient for the nonisothermal system, $C_{D'}$, was calculated from an expression given by Lewis and Gauvin.[2]

$$C_{D'}/C_{D,av} = (\nu_{g,av}/\nu_{g,e})^{0.15} \quad [13]$$

The dependence of C_D upon particle Reynolds number was taken from a correlation given by Beard and Pruppacher.[11]

The validity of using a history term which was originally derived for creeping flow as well as the validity of the assumption that the motion of the particle is determined by the mean flow rather than the turbulent fluctuations has been discussed by Lewis and Gauvin.[2] Although these questions are by no means settled, our rationale for taking this approach is that past work[1,2,4] has shown that these assumptions give quite good agreement with experimental measurements.

In Eq. [13] the subscripts e and av refer to gas property values at the edge of the boundary layer around the particle and at the mean film temperature, $T_{g,av}$, across the boundary layer, respectively, *i.e.*,

$$T_{g,av} = (T_{g,e} - T_p)/2 \quad [14]$$

The particle temperature was calculated from

$$\frac{d}{dt}(Q_p) = \mathrm{Nu} K_{g,av} \pi D_p (T_{g,e} - T_p) \quad [15]$$

where Q_p is the heat content of the particle and where it is assumed that the interior of the particle is at a uniform temperature. In this equation particle heating by radiation has been neglected and it was found that radiative losses from the particle were negligible.

The Nusselt number, Nu, was taken from a correlation proposed by Ranz and Marshall:[12]

$$\mathrm{Nu} = 2 + 0.6\, \mathrm{Re}^{0.5} \sigma_{T,g}^{0.33} \quad [16]$$

and was corrected for nonisothermal conditions in the same manner as the drag coefficient, *i.e.*,

$$\mathrm{Nu}'/\mathrm{Nu}_{av} = (\nu_{g,av}/\nu_{g,e})^{0.15} \quad [17]$$

Equations [12] to [17] were solved numerically using a fourth order Runge-Kutta technique. The solutions thus obtained then gave the temperature and heat content of the particles as a function of their position within the plasma flame.

C. *Heat Transfer and Solidification during Plasma Spraying*

Plasma spraying is a classical moving boundary problem where the outer surface of the deposit advances with a constant velocity determined by the spraying rate. The temperature history of the sprayed particles in the plasma as well as the heat transfer from the particles to the target plays a key role in process control and deposition quality.

The conservation of thermal energy within the substrate and the coating is governed by the time dependent heat conduction equation which may be expressed in one-dimensional form as:

$$\frac{\partial T_c}{\partial t} + U_c \frac{\partial T_c}{\partial x'} = \frac{\partial}{\partial x'} \left(\alpha_c \frac{\partial T_c}{\partial x'} \right) \quad [18]$$

In this equation the subscript c may refer to the solid coating or the target material as appropriate. The above equation is the heat conduction equation expressed in terms of a transformed coordinate x' whose origin corresponds to the surface of the deposit which is moving upward at a constant spray velocity U_c (Figure 2). For heat transfer to the substrate in the absence of particles, $U_c = 0$. For the purposes of deriving Eq. [18] it was assumed that the spray velocity was independent of the radial coordinate, *i.e.*, that the particles are uniformly distributed in the jet at the point of impact. In practice, the particles will not be distributed uniformly and U_c will be a function of r. The derivation of the relevant heat conduction equation for this case is given in Appendix 2.

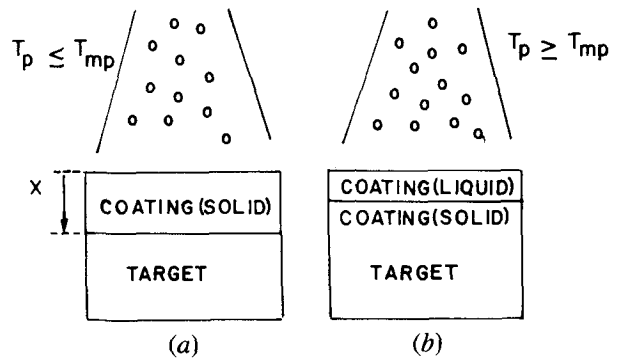

Fig. 2—Schematic representation of deposition buildup.

The boundary condition describing the heat flux from the plasma to the substrate or coating ($x' = 0$) is given as

$$-K_c \frac{\partial T_c}{\partial x'} = q_t + \rho_c \frac{Q_p}{M_p} U_c \qquad [19]$$

In Eq. [19], q_t now includes the radiative transfer from the plasma to the target. Radiative losses by the target were neglected since they are small over the majority of the surface of the target and small in comparison to the plasma and particle heating in the impingement zone.

Equations [18] and [19] are the basic equations to be solved in order to evaluate the temperature field in the target and in the deposited material and, consequently, the solidification rate. Since the relationship between the process variables and the physical picture of the solidification process is not readily apparent from the form of the equations, it is informative to obtain an approximate analytic solution of the one-dimensional problem.

When the particles, or droplets, are being deposited there are two distinct physical situations to be considered depending upon whether the particle temperature is below or above its melting point. In the former case the spraying process is characterized by the deposition of a solid phase on the target as sketched in Figure 2(a). Under these conditions deposition buildup can proceed to any thickness as long as it satisfies the adhesion criteria which depend on the properties of the impinging particles, and their temperature and momentum. When the temperature of the sprayed particle is at or above its melting point the physical picture may be changed by the presence of a liquid layer in addition to the solidified sprayed material on top of the target. This situation is illustrated in Figure 2(b).

An approximate description of the solidification problem may be obtained by considering a related one-dimensional Stefan problem. For a semi-infinite liquid, initially at its melting temperature, in contact with a semi-infinite solid, the motion of the solidification front into the liquid is given by the following equation:[13]

$$X(t) = 2\eta^*(t\alpha_c)^{0.5} \qquad [20]$$

The solidification rate is parabolic in time. The solidification rate constant, η^*, may be calculated from

$$\frac{\exp(-\eta^{*2})}{(S^*)^{-0.5} + \operatorname{erf}(\eta^*)} = \pi^{0.5} L^* \eta^* \qquad [21]$$

where $S^* = \rho_s C_s K_s / \rho_c C_c K_c$ is the ratio of the thermal and physical properties of the substrate and the sprayed coating. The dimensionless latent heat of the coating, L^*, is defined as $L^* = L_c / C_c (T_{mp} - T_{i,s})$ where T_{mp} is the particle melting point and $T_{i,s}$ is the initial temperature of the substrate.

Figure 3 shows a sketch of the growth rate of the solidified layer. This is initially very rapid as a result of the high temperature gradient at the interface between the coating and the target. For comparison, the growth rate of the deposit thickness for plasma spraying is included, and it is seen that the surface of the deposit advances at a constant velocity resulting in the straight line shown in Figure 3. For a high spraying rate (case 1) the thickness of the solidified layer is always less than that of the deposited layer, and the deposit/plasma interface is maintained in a liquid state. In other words, the rate of energy supply by the particles is greater than the rate of heat extraction by the substrate and,

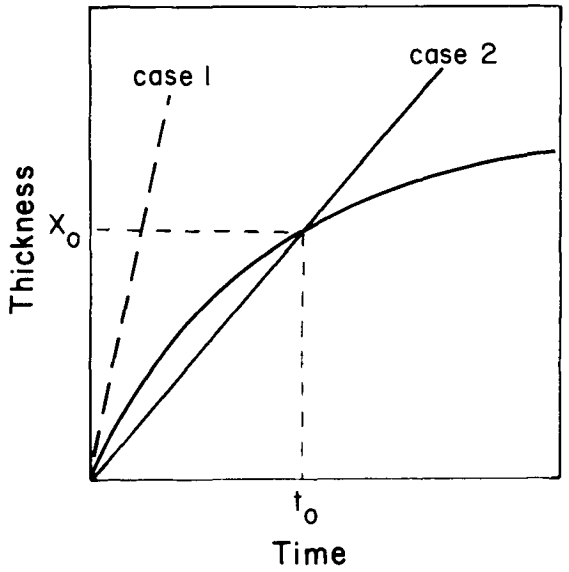

Fig. 3 — Sketch of solidification rate and spraying rate as predicted by the 1-dimensional approximate analytic solution.

hence, the rate of solidification is solely determined by the rate of heat extraction by the target. Under these conditions the deposit may consist of a solid and a molten layer. The fact that the molten layer may be at least partially blown away by the impinging jet makes this mode of operation unsatisfactory. The temperature fields in the substrate and the solidified layer are:

$$T_s^* = \frac{1 - \operatorname{erf}(\lambda^*)}{1 + (S^*)^{0.5} \operatorname{erf}(\eta^*)} \qquad [22]$$

$$T_c^* = \frac{1 + (S^*)^{0.5} \operatorname{erf}(\lambda^*)}{1 + (S^*)^{0.5} \operatorname{erf}(\eta^*)} \qquad [23]$$

respectively, where $T^* = (T - T_{i,s})/(T_{mp} - T_{i,s})$ is the dimensionless temperature and $\lambda^* = |x|/2(\alpha t)^{0.5}$ is the dimensionless distance from the target/coating interface in the direction of propagation of the solidification front.

At low spraying rates (case 2) the initial solidification rate is higher than the deposition rate. At time t_0 the solidified thickness is equal to the thickness of the deposited layer, while for times later than t_0 the solidified layer thickness, X_0, is less than the deposit thickness. It is clear that below X_0 the rate of heat extraction by the substrate is higher than the energy supplied by the particles; that is, the sprayed liquid particles will be rapidly solidified upon impact and the deposition will be similar to the case of the spraying of solid particles shown in Figure 2(a). The cooling rate may be obtained by solving for the temperature distribution in the solid deposit. For X greater than X_0 a liquid phase will appear above the solid deposit and the solidification rate is controlled by the heat extraction of the substrate. As we can see, the rate of buildup of the liquid layer increases with time.

In practice the presence of a liquid layer is not desirable if a controlled solidification rate is to be achieved since the thickness of the solid deposit is less than or equal to X_0. (It should be emphasized that, in reality, the depth of the solid layer can never be greater than the total thickness of the coating and only arises here since we are calculating solidification into a semi-infinite liquid. Nevertheless, this

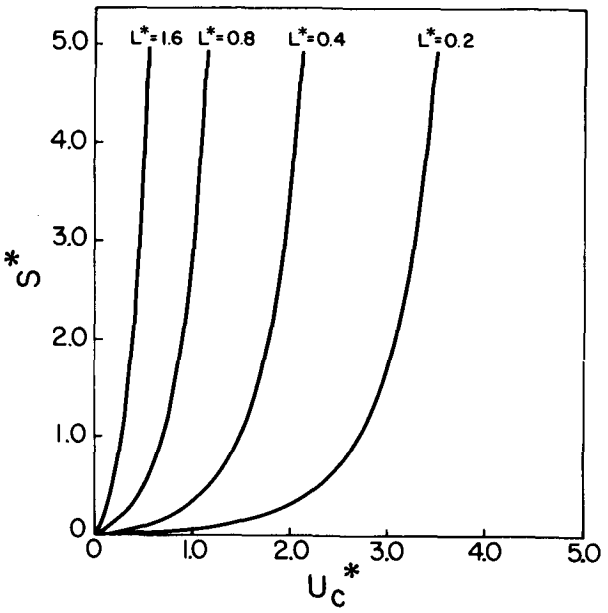

Fig. 4—Dependence of dimensionless spray velocity on substrate and coating properties and particle latent heat.

approach is useful since it allows us to obtain an approximate idea of the thickness of the solidified layer that may be obtained before a liquid layer forms, and to contrast the markedly different behavior between the aluminum and nickel particles.)

To obtain an approximate idea of the thickness, X_0, of the solidified material during the initial period as a function of the spraying parameters it is useful to define the dimensionless spraying velocity, $U_c^* = U_c X_0/\alpha_c$.

Figure 4 shows the dependence of U_c^* upon the properties of the deposit and the substrate, S^*, as a function of the dimensionless latent heat L^* (which itself is a function of the initial substrate temperature). It is seen that U_c^* is independent of S^* above a value of 1.0 and very strongly dependent on the dimensionless latent heat since for high S^* the main resistance to heat flow is due to the solidifying material. The practical importance of this figure is that for any particle or target material, defined by S^*, and a given L^*, U_c^* may be obtained and hence X_0 may be calculated for any given spray velocity.

The above analysis gives a clear understanding of solidification and heat flow problems in plasma spraying as well as an approximate quantitative analysis. For accurate calculations of real problems with different values of the particle superheat it is necessary to resort to numerical techniques.

III. COMPUTED RESULTS

In the previous section we presented a general formulation describing the plasma spray deposition process, the key components of which included:

1. the characterization of the plasma jet,
2. the plasma jet/particle interaction, and
3. the heat transfer phenomena in the deposit and the substrate.

In addition, certain approximate solutions were presented, primarily to illustrate the general behavior of these systems. In the present section we shall describe a selection of the computed results and, wherever possible, these will be compared with experimental measurements.

A. *Plasma Jet Behavior*

While a great deal of work has been done on the modeling of heat transfer and fluid flow in plasma jets, only very recently have really accurate experimental measurements become available for the critical testing of these predictions.

Figures 5 and 6 show a comparison between the experimentally measured velocity and temperature fields in a plasma jet reported by Fauchais and co-workers[1] with predictions based on the model described in Section II.[6] It is seen that the agreement is quite good, providing direct verification regarding the appropriateness of the model employed.

The operating parameters of the plasma spray system modeled in the current work are given in Table I along with the estimated values of velocity and temperature at the torch

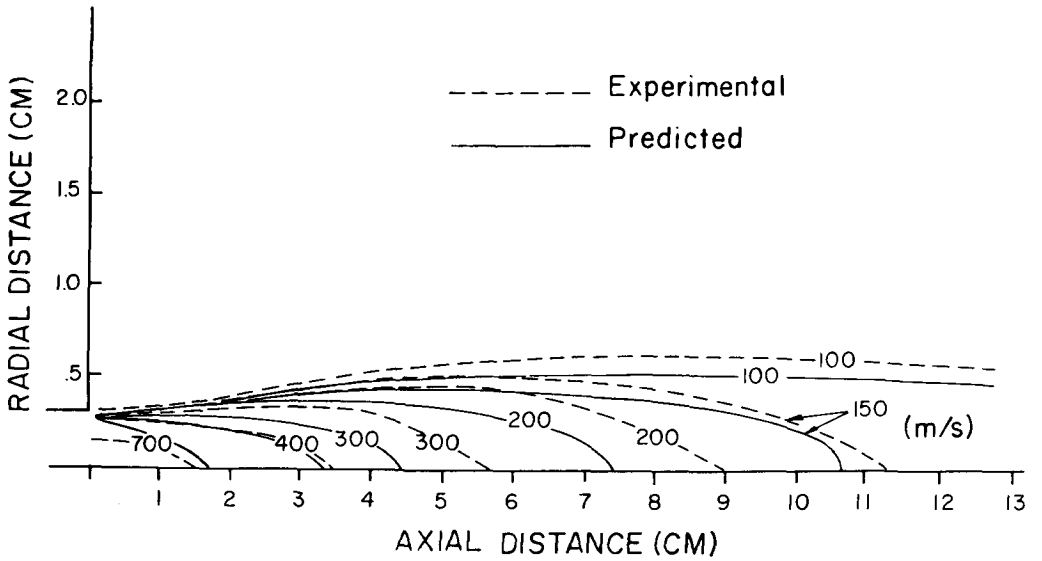

Fig. 5—Comparison between predicted[6] and measured[1] velocity fields for an argon/hydrogen plasma.

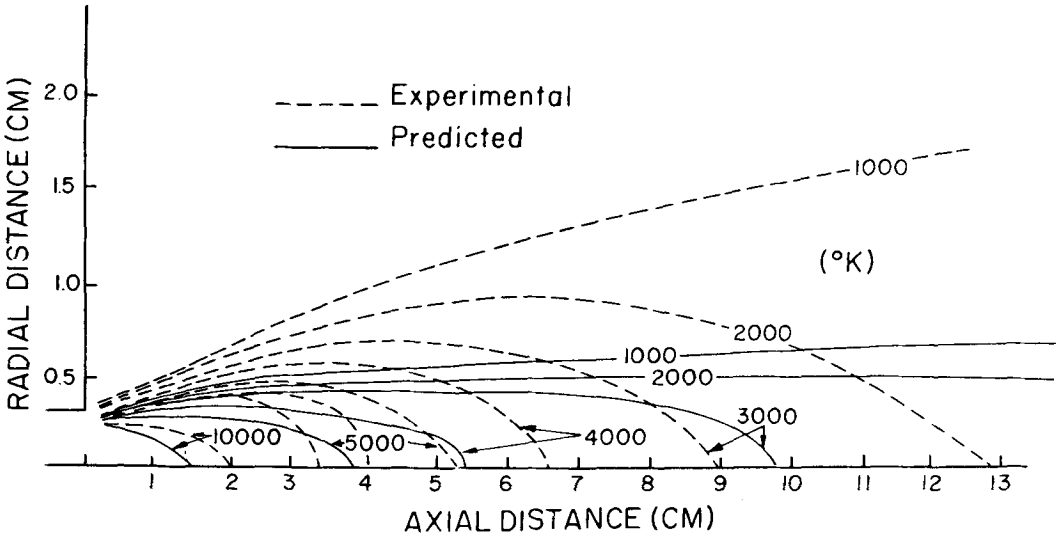

Fig. 6—Comparison between predicted[6] and measured[1] temperature field for an argon/hydrogen plasma.

Table I. Process Parameters for Plasma Spray System

Working gas	argon
Arc current	700 A
Arc voltage	30 V
Gas flow rate	786.6 cc/s
Nozzle I.D.	12.7 mm
Torch target separation	76 mm and 100 mm
Exit velocity of gas	223 meters/sec
Exit temperature of gas	10,000 K
Aluminum particle diameter	150 μm
Nickel particle diameter	75 μm
Target material	copper
Target diameter	130 mm
Target thickness	38 mm

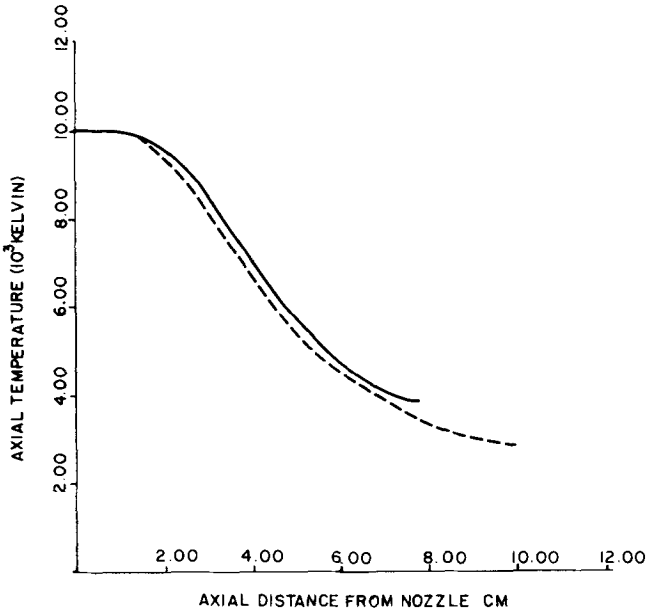

Fig. 8—Predicted axial temperatures for 2 torch/target separations. 76.2 mm (solid), 100 mm (broken).

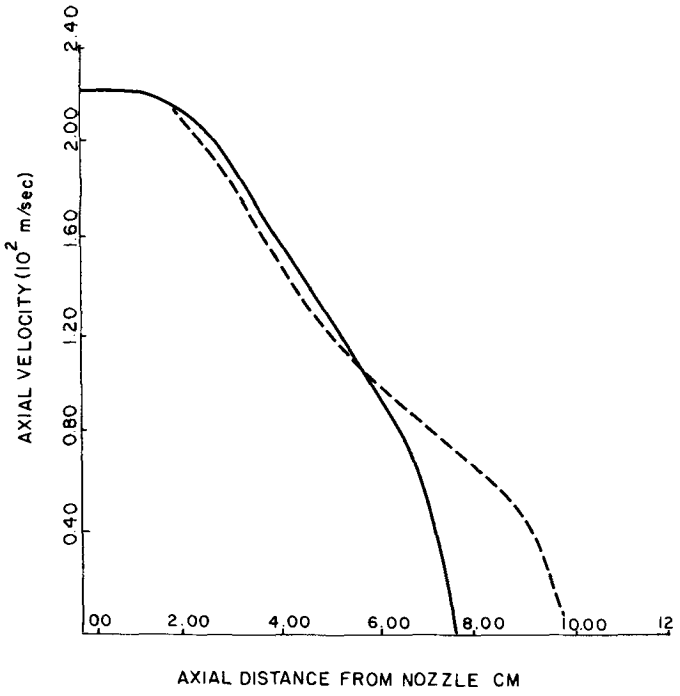

Fig. 7—Predicted axial velocity in plasma for 2 torch/target separations. 76.2 mm (solid), 100 mm (broken).

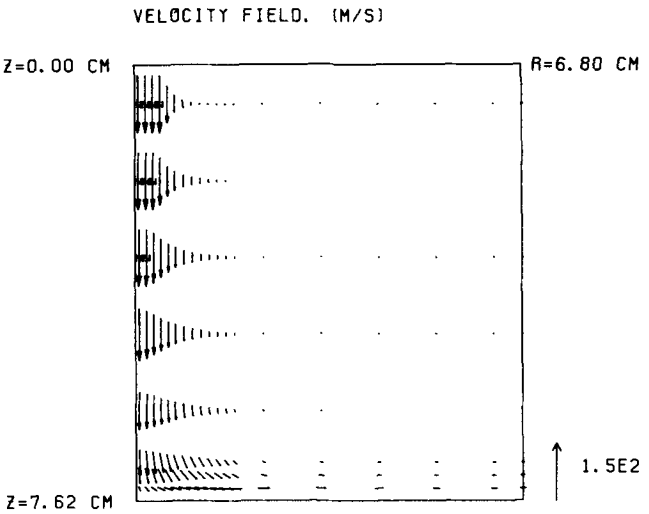

Fig. 9—Predicted plasma velocity field for 76.2 mm torch/target separation.

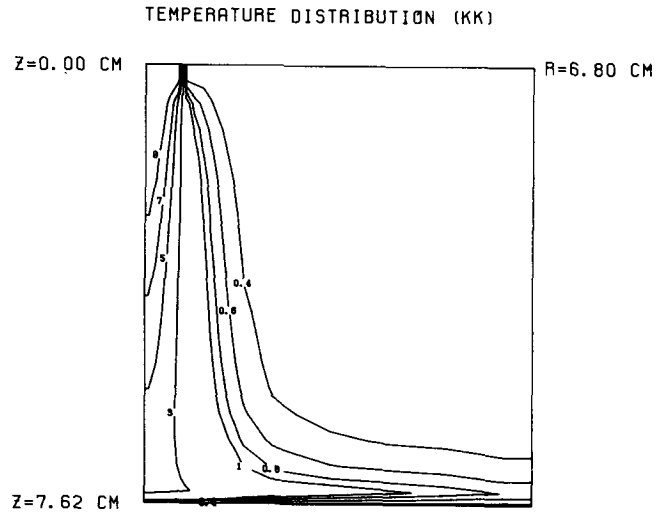

Fig. 10—Predicted plasma temperature field for 76.2 mm torch/target separation.

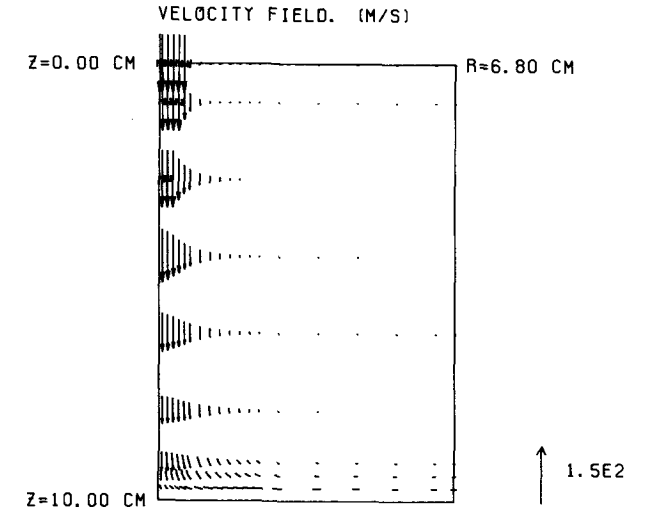

Fig. 11—Predicted plasma velocity field for 100 mm torch/target separation.

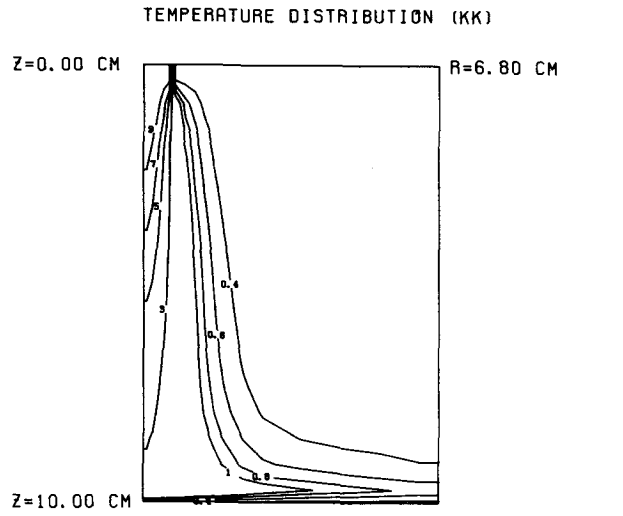

Fig. 12—Predicted plasma temperature field for 100 mm torch/target separation.

exit. The predicted profiles of axial velocity and temperature for two different torch/target separations are shown in Figures 7 and 8. It is seen that while the presence of the target does indeed modify the temperature and velocity profiles, these effects are confined to a region in the vicinity of the target. This is further illustrated by Figures 9 to 12 which show the corresponding velocity and temperature fields. The temperature distributions given in Figures 11 and 12 exhibit quite clearly a constant temperature core in the flow development region followed by a rapid temperature decrease as the target is approached.

The heat transfer from the plasma to the target is determined from calculated values of the plasma temperature at the edge of the target boundary layer and from the calculated values of the heat transfer coefficient across the boundary layer using Eqs. [10] and [11]. The predicted values of $T_{g,b}$ and h for the two torch target separations are shown in Figures 13 and 14.

B. *Plasma Jet/Particle Interaction*

The first step in assessing the heat transfer between the plasma jet and the injected particles is to compute the particle trajectory and residence time. These quantities will necessarily depend upon the location and the speed with which the particles are injected into the plasma jet. For the system considered here insufficient data were available on the actual injection parameters of the particles, and it was necessary to assume that they started from rest at the nozzle exit and were initially at room temperature.

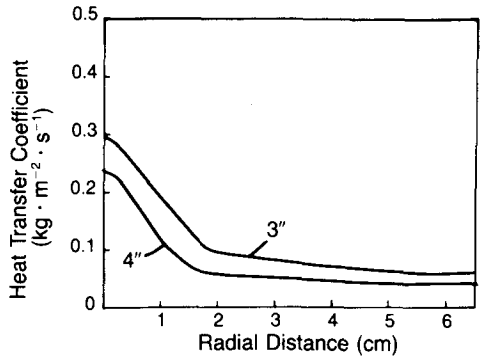

Fig. 13—Predicted heat transfer coefficient for heat transfer from the plasma to the target.

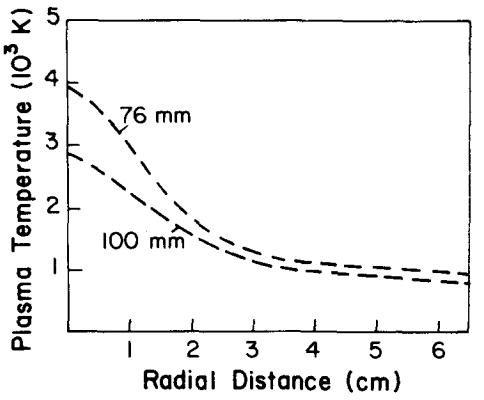

Fig. 14—Predicted plasma temperature at the edge of the target boundary layer in the plasma.

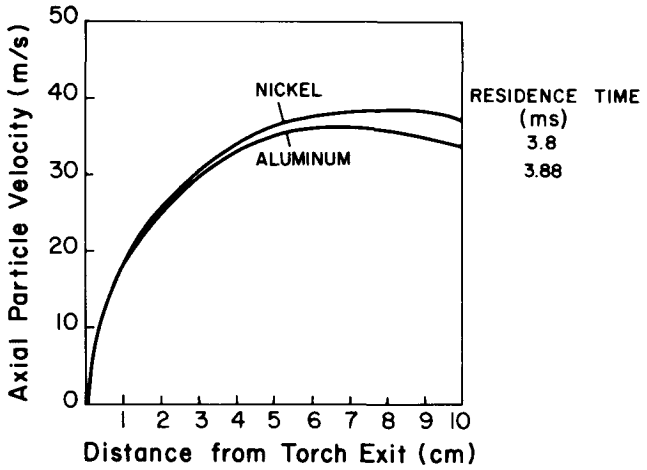

Fig. 15—Predicted particle velocity for motion along the centerline of the jet.

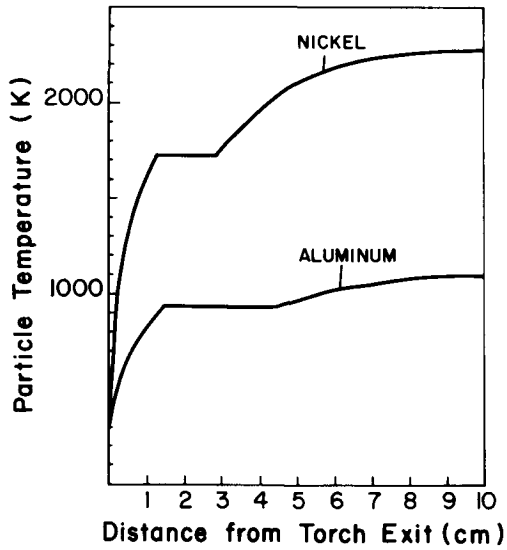

Fig. 16—Predicted particle temperature for motion along the centerline of the jet.

Figure 15 shows the predicted particle velocities for motion along the centerline of the jet for nickel spheres of 75 μm diameter and aluminum spheres of 150 μm diameter. The particles attain maximum velocities of 35 to 40 m/s and have residence times in the plasma of about 4 ms. Figure 16 shows the corresponding particle temperatures; it is seen that both the nickel and aluminum particles become fully molten and that most of the heat transfer takes place in the jet core in the vicinity of the exit from the gun. An experimental confirmation of these results would be very desirable.

C. *Heat Transfer in the Substrate and the Deposit*

1. *Heat flow in the deposit*

Calculations of heat transfer in the target (or substrate) were initially performed for target heating in the absence of particles. In this case the target was a copper disk and the only heating came directly from the plasma jet. Figure 17 shows a comparison between the experimentally measured[14]

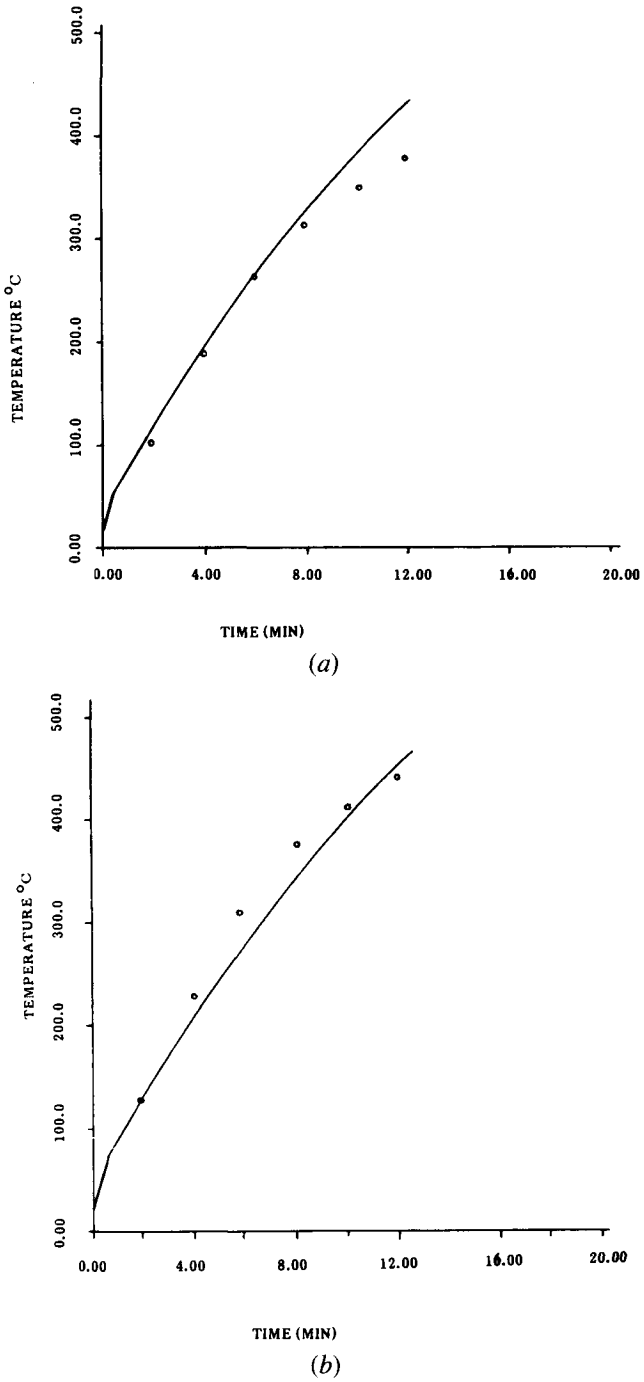

Fig. 17—Comparison between the predicted and measured[14] temperature rise in the target at the point of impingement of the plasma jet when there are no particles being sprayed. (*a*) 76 mm torch/target separation, (*b*) 100 mm.

(discrete data points) and the theoretically predicted temperature rise at the center of the target. The calculations and experiments were performed for the operational parameters given in Table I. The very good agreement between theory and experiment provides further proof regarding the appropriateness of the plasma model.

Figure 18 shows the computed heat transfer to the target as a function of time. It is interesting to note that the total heat transfer for the 76 mm and 100 mm cases is almost the same. This is consistent with the computed values of plasma

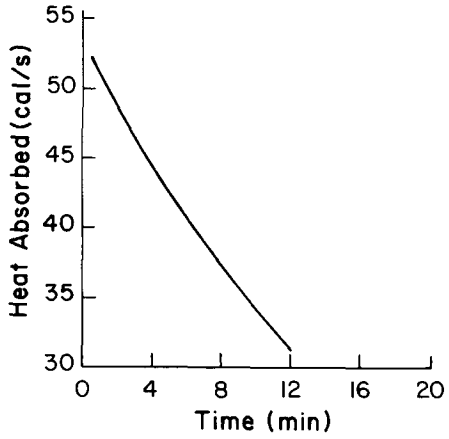

(a)

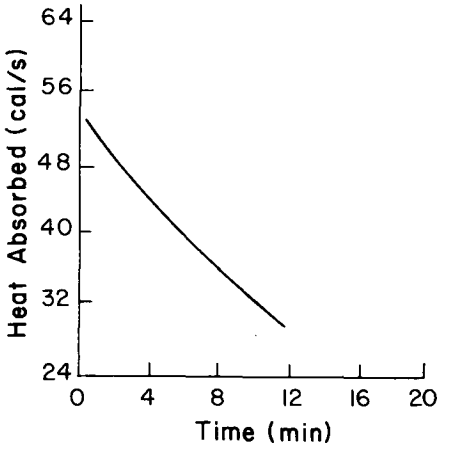

(b)

Fig. 18 — Predicted heat absorbed by target from plasma jet (no particles). (*a*) 76.2 mm torch/target separation, (*b*) 100 mm.

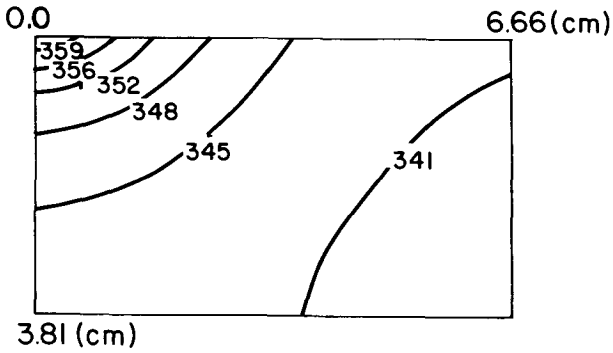

Fig. 19 — Predicted target isotherms after 9 min for 76.2 mm torch/target separation (no particles).

temperature and heat transfer coefficient given in Figures 13 and 14 where the major difference between the 76 mm and 100 mm cases is restricted to the first 2 cms nearest the center of the target — a region only 10 pct of the total target area.

Figure 19 shows the computed temperature field in the target after 9 minutes for the 100 mm torch target separation. The temperature of the target is almost uniform which may be attributed to the high thermal conductivity of copper. This finding is in agreement with experimental measurements.[13]

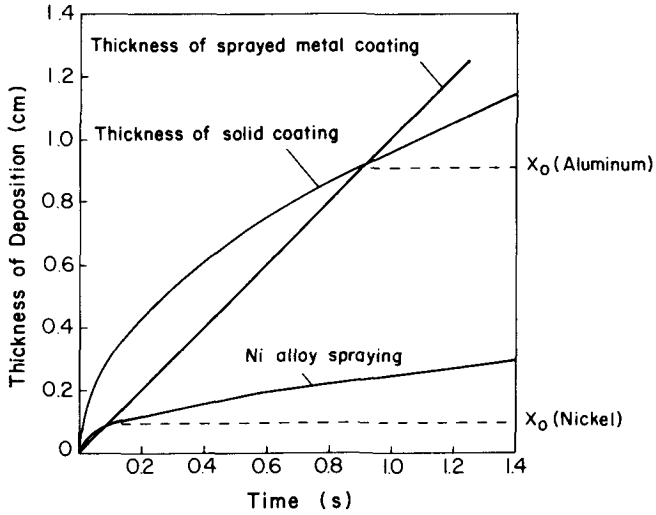

Fig. 20 — Solidification rates for aluminum and nickel spraying predicted using simple 1-dimensional analytical model.

2. *Substrate heating*

As was described earlier (Section II-C) in the presence of sprayed particles the intersection of the solidification curve (Figure 3) with the spray rate defines the limiting conditions for satisfactory operation since once the spray rate exceeds the solidification rate a liquid film is formed.

Figure 20 shows the solidification rate for aluminum and nickel sprayed onto a copper target together with the constant spray rate of 10 mm per second. The region to the left of the intersection of these two curves defines the realm of satisfactory operation. It is seen that a fairly thick aluminum deposit may be formed but that the thickness of the nickel coating that may be obtained is limited to about 1 mm. This behavior is readily explained by the fact that the nickel particles carry a much higher enthalpy and, at the same time, the lower thermal conductivity of the nickel layer prevents the effective dissipation of this thermal energy. These calculations assume that the thermal conductivity, density, and specific heat of the coating are equal to those of the particles, which may not be true for porous coatings. In principle it would be possible to account for porosity by assigning effective values to these thermal and physical properties.

It should be stressed that while the analytical solution given by Figure 20 provides a useful insight into the behavior of the system, important simplifying assumptions have been made in its development. In particular it is assumed that the solidification front advances into a liquid of infinite extent while, in reality, its movement is limited by the total depth of coating which is defined by the spraying velocity U_c. For the accurate representation of real systems numerical techniques are required, and it is no longer necessary to specify that the outer surface of the deposit is at the melting temperature. Figure 21 shows the ratio of the numerically computed values of X_0 (using Eqs. [18] and [19]) to the analytically predicted values for different values of the particle superheat $H^* = (T_p - T_{mp})/(T_{mp} - T_{i,s})$. For aluminum and nickel spraying this ratio is about 0.6 at zero particle superheat. This roughly corresponds to the point where the solidification rate equals the spraying rate. The predicted thickness of the rapidly solidified layer is strongly reduced by particle superheat.

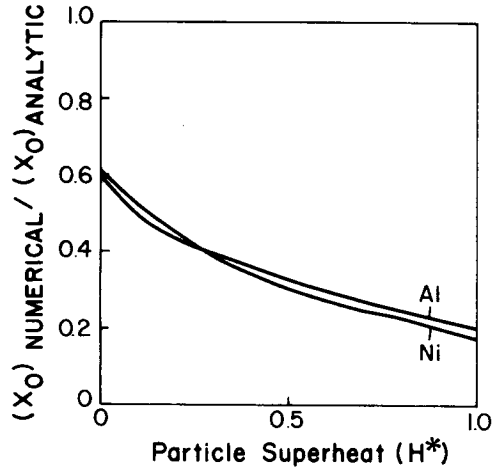

Fig. 21 — Comparison between the values of X_0 predicted using the numerical model and those predicted using the simple 1-dimensional analytical model of solidification.

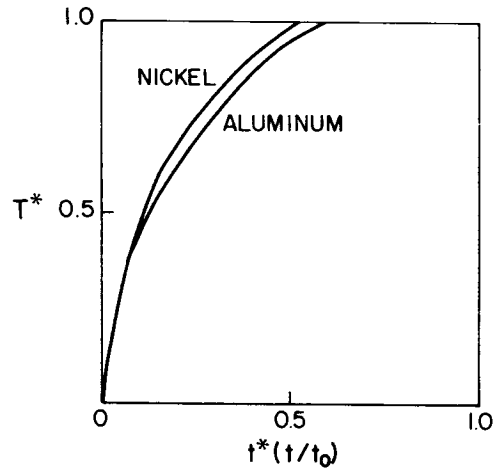

Fig. 22 — Predicted temperature history of the surface of the solid coating.

Figure 22 shows the dimensionless temperature of the deposit surface as a function of time for nickel and aluminum spraying for zero superheat. During the initial period the sprayed particles are rapidly quenched to a low temperature. As the thickness of the deposit increases, its surface temperature rises to its melting point. The importance of this curve lies in the fact that it may be used to determine the cooling rate of the sprayed particles which is one of the more important parameters for characterizing the structure of the solidified layer. As expected, the structure may vary significantly with position in the solidified layer.

In deducing quantitative values for the cooling rate from Figure 22, it is necessary to realize that this dimensionless plot represents the temperature history at the outer edge of the deposit. It follows that the quenching rate will be progressively reduced with the buildup of the material, with the attainment of $T^* = 1$ signaling the establishment of a liquid film.

While the specific quench rate at the particle level may be described only through the detailed consideration of particle impact and deformation, the following approximate relationship may be employed to estimate the quench rate on a continuum basis:

$$\text{Quench rate} \simeq (1 - T^*)(T_{mp} - T_{i,s})\, U_c/D_p \qquad [24]$$

The maximum quench rate, corresponding to $t^* \to 0$, is then given by $(T_{mp} - T_{i,s})\, U_c/D_p$ which for the conditions considered would be about 2.0×10^5 °C per second for nickel and 5.0×10^4 °C per second for aluminum. These values are within the range expected for rapid solidification processes.[15]

The very important point that has to be made as a result of these calculations is that one may vary the solidification rate obtainable, and hence control the structure of the deposit, by varying the spraying conditions. The model developed here allows one to quantify these relationships.

IV. DISCUSSION

In the paper, a mathematical representation has been developed describing the plasma spraying process, in which allowance has been made for the fluid flow and temperature fields in the plasma jet, the plasma/particle interaction, and the heat transfer phenomena associated with the deposition process. As a result it was possible to predict the particle residence time in the plasma, the temperature history of the particles, and the temperature history of the deposit formed.

Perhaps the most important finding reported in this paper was that on the basis of the heat transfer analysis one may define the limiting conditions for satisfactory operation of the deposition process. More specifically, one pre-condition for the formation of a coherent nonporous deposit is that the particles should arrive at the substrate in a molten state. The other limiting condition is that the rate of heat extraction by the substrate should be sufficiently high that a solid rather than a molten deposit is formed. Clearly, this condition is established by balancing the rate of heat supply (*i.e.*, the spray rate and the superheat of the arriving particles) against the rate of heat extraction, which will necessarily diminish with the buildup of the deposit.

In all modeling efforts it is desirable to compare the predictions with measurements. In the present case such a comparison could be made with reported work concerning heat and fluid flow phenomena in plasma systems and plasma jet/target interactions. The predictions regarding deposit morphology have not yet been confirmed on a quantitative basis, but appear to be consistent with experimental observations.

At this stage it is worthwhile to delineate what has been the novel contribution of this work. While a great deal of useful work has been done on the modeling of plasma spray systems by Gauvin,[2,3] Boulos,[4] and Fauchais,[1] this work has not considered the plasma jet/target interaction or the deposition buildup and solidification. In contrast, the current work has given a quantitative description of the impinging plasma jet using only basic process parameters as input data and has quantified both the plasma/particle interaction and the heat transfer and solidification phenomena associated with the deposition as well as defining the conditions for satisfactory operation. It should be stressed that the approach described here has to be regarded as the beginning of a program of research which could be substantially extended, preferably by a combination of experimental and theoretical work. It would be desirable to carry out plasma spraying experiments using proper diagnostic facilities to

verify the predictions made for particle velocities, trajectories, and temperatures. Such work, in combination with the detailed structural characterization of the deposit and measurement of its thermal history, should provide a satisfactory basis for the extension of the theory. Future theoretical work should also include the assessment of the spatial distribution of the particles, the consideration of a two-way interaction between the plasma jet and the particles, and the examination of the microscopic aspects of the deposition process.

APPENDIX 1

Outline of the k-ε turbulence model

The k-ε model of turbulence postulates that the turbulent viscosity, μ_{eff}, is given by the following relationship:

$$\mu_t = C_3 \rho \frac{k^2}{\varepsilon} \qquad [A1]$$

where k is the turbulent kinetic energy of the fluid and ε is the rate of dissipation of k. (C_3 is a constant.)

The turbulence quantities k and ε are obtained through the solution of conservation equations which take the form

$$\frac{\partial}{\partial z}(\rho_g u_g \phi) + \frac{1}{r}\frac{\partial}{\partial r}(\rho_g r v_g \phi) = \frac{\partial}{\partial z}\left(\frac{\mu_{\text{eff}}}{\sigma}\frac{\partial \phi}{\partial z}\right) + \frac{1}{r}\frac{\partial}{\partial r}\left(\frac{\mu_{\text{eff}}}{\sigma}\frac{r\partial \phi}{\partial r}\right) + S \qquad [A2]$$

where S is the net rate of generation of the turbulent properties per unit volume.

For the k equation

$$S = G - \rho_g \varepsilon \qquad [A3]$$

and for ε

$$S = C_1 \frac{\varepsilon}{k} G - C_2 \frac{\varepsilon^2}{k} \rho_g \qquad [A4]$$

The generation of turbulence is given by

$$G = 2\mu_t \left\{ \left(\frac{\partial u_g}{\partial z}\right)^2 + \left(\frac{\partial v_g}{\partial r}\right)^2 + \left(\frac{v_g}{r}\right)^2 + \frac{1}{2}\left(\frac{\partial v_g}{\partial z} + \frac{\partial u_g}{\partial r}\right)^2 \right\} \qquad [A5]$$

It follows that ultimately the solution of the fluid flow problem requires the simultaneous solution of six transport equations, namely: continuity, two momentum equations, equations for k and ε, and the energy equation. In addition, the numerical values chosen will depend upon the values chosen for the constants C_1, C_2, C_3, and the Prandtl numbers, σ, for T, k, and ε. The values used in the present model are taken from Pun and Spalding[10] and are given in Table II.

Table II. Values of Constants Used in Two-Equation Turbulence Model

C_1	1.43
C_2	1.92
C_D	0.09
σ_k	1.0
$\sigma\varepsilon$	1.3
σ_T	0.9

APPENDIX 2

Heat conduction equation for two-dimensional spraying

In Section II-C the one-dimensional heat conduction equation was used to calculate the temperature fields in the target and the sprayed coating. The moving boundary resulting from the growth of the coating was dealt with by transforming to a coordinate system whose origin was stationary with respect to the surface of the coating. It is known from experiments[14] that the one-dimensional assumption is an over-simplification since there exists a nonuniform distribution of particles in the jet. In this case the situation is further complicated since the moving boundary corresponding to the solid/plasma interface now has an irregular shape.

The two-dimensional heat conduction equation may be written as follows:

$$\frac{\partial T}{\partial t} = \frac{\partial}{\partial x}\left(\alpha \frac{\partial T}{\partial x}\right) + \frac{1}{r}\frac{\partial}{\partial r}\left(\alpha r \frac{\partial T}{\partial r}\right) \qquad [A6]$$

In this equation x is the axial coordinate in the substrate whose origin is fixed at the interface between the target and the sprayed coating.

Let us now define a new coordinate, x', by the following relationship:

$$x' = [x + U(r)t]/[U(r)t] \qquad [A7]$$

The origin of the coordinate system has been shifted to the surface of the sprayed coating ($x' = 0$) and has been stretched so that the coating/substrate interface is defined by $x' = 1$.

In the transformed coordinate system the heat conduction equation takes the form:

$$\frac{\partial T}{\partial t} + \left(\frac{1 - x'}{t}\right)\frac{\partial T}{\partial x'} = \frac{1}{X^2}\frac{\partial}{\partial x'}\left(\alpha \frac{\partial T}{\partial x'}\right) + \frac{1}{r}\frac{\partial}{\partial r}\left(r\alpha \frac{\partial T}{\partial r}\right) + \left(\frac{1 - x'}{r}\right)\frac{\partial}{\partial r}\left(\frac{r}{U}\alpha \frac{dU}{dr}\frac{\partial T}{\partial x'}\right) + \frac{dU}{dr}\left(\frac{1 - x'}{U}\right)\frac{\partial}{\partial x'} \cdot \left(\alpha \frac{\partial T}{\partial r}\right) + \left(\frac{dU}{dr}\frac{1}{U}\right)^2 (1 - x')\frac{\partial}{\partial x'}\left\{\alpha(1 - x')\frac{\partial T}{\partial x'}\right\} \qquad [A8]$$

where $X(r, t)$ is the thickness of the solid coating.

Despite its complicated appearance, Eq. [A8] is readily amenable to numerical techniques and has an advantage over Eq. [A6] in that the boundary conditions are specified on plane surfaces at $x' = 0$ and $x' = 1$. Boundary conditions at the lower surface of the substrate are replaced by conditions at $x' = \infty$, based upon the assumption that the thickness of the target is greater than the penetration thickness of the temperature field in the time considered.

NOTATION

C Specific heat
C_1 to C_3 Constants in turbulence model

C_D	Drag coefficient
C_D'	Drag coefficient modified for nonisothermal conditions
D	Diameter
h	Heat transfer coefficient from plasma to target
H^*	Particle superheat
k	Turbulent kinetic energy per unit volume
K	Thermal conductivity
L	Latent heat of sprayed material
L^*	Dimensionless latent heat of particle
M	Mass
Nu	Nusselt number
P	Pressure
q_t	Heat flux from plasma jet to target
Q	Heat content
r	Radial coordinate (distance from axis of symmetry)
R	Radius
Re	Particle Reynolds number
S	Source term in conservation equations
S^*	Ratio of coating and substrate properties
t	Time
T	Temperature
u	Axial velocity
U, U_c	Spray velocity (rate of increase of coating thickness)
v	Radial velocity
x	Axial coordinate in target (origin at target/coating interface)
x'	Axial coordinate in target (origin at surface of coating)
X	Coating thickness
X_0	Thickness of solid coating when liquid layer appears
Y	Thickness of coating + thickness of target
z	Axial coordinate (origin at torch exit)
α	Thermal diffusivity
ε	Dissipation rate of turbulence energy
η^*	Solidification rate constant
μ	Viscosity (molecular viscosity if no subscript attached)
ν	Kinematic viscosity
ρ	Density
σ	Prandtl number

Subscripts

av	Property value at mean film temperature
b	Value at edge of boundary layer in plasma
c	Coating
e	Value at edge of boundary layer around particle
eff	Effective
g	Gas (plasma)
mp	Melting point of particle
p	Particle
R	Radiation
s	Substrate (target)
t	Turbulent
T	Temperature
w	Wall (surface of solid target or solid coating)
0	Value at torch exit (for plasma model)

ACKNOWLEDGMENTS

The authors wish to thank TRW Inc. for the support of this investigation, and thanks are due to Dr. T. Piwonka and Stephan Murphy for helpful discussions.

REFERENCES

1. A. Vardelle, M. Vardelle, and P. Fauchais: *Plasma Chem. & Plasma Process.*, 1982, vol. 2, pp. 255-91.
2. J. A. Lewis and W. H. Gauvin: *A.I.Ch.E. Jnl.*, 1973, vol. 19, pp. 982-90.
3. D. Bhattacharyya and W. H. Gauvin: *A.I.Ch.E. Jnl.*, 1975, vol. 21, pp. 879-85.
4. M. I. Boulos and W. H. Gauvin: *Can. Jnl. Chem. Engng.*, 1974, vol. 52, pp. 355-63.
5. E. R. Eckert and E. Pfender: *Advances in Heat Transfer*, Academic Press, New York, NY, 1967, vol. 4, pp. 229-316.
6. J. McKelliget, J. Szekely, M. Vardelle, and P. Fauchais: *Plasma Chem. & Plasma Process.*, 1982, vol. 2, pp. 317-32.
7. B. F. Launder and D. B. Spalding: *Comp. Meth. in Appl. Mech. Engng.*, 1974, vol. 3, pp. 269-89.
8. C. Liu: Ph.D. Thesis, University of Minnesota, Minneapolis, MN, 1977.
9. D. L. Evans and R. S. Tankin: *Phys. Fluids*, 1967, vol. 10, pp. 1137-44.
10. W. M. Pun and D. B. Spalding: Report# HTS/76/2, Heat Transfer Section, Imperial College, Exhibition Road, London, 1976.
11. K. V. Beard and H. R. Pruppacher: *Jnl. Atmos. Sci.*, 1969, vol. 26, p. 1066.
12. W. E. Ranz and W. R. Marshall: *Chem. Engng. Progr.*, 1952, vol. 48, pp. 141-46, 173-80.
13. W. M. Rosenow and J. P. Hartnett: *Handbook of Heat Transfer*, McGraw-Hill, 1973, p. 3.93.
14. S. D. Murphy: "Flexible Manufacturing", Interim Engineering Report, ER-8204-1, TRW Equipment Group, Material Technology Division, 23555 Euclid Ave., Cleveland, OH, 1981-2.
15. K. Myazawa and J. Szekely: *Metall. Trans. A*, 1981, vol. 12A, pp. 1047-57.